

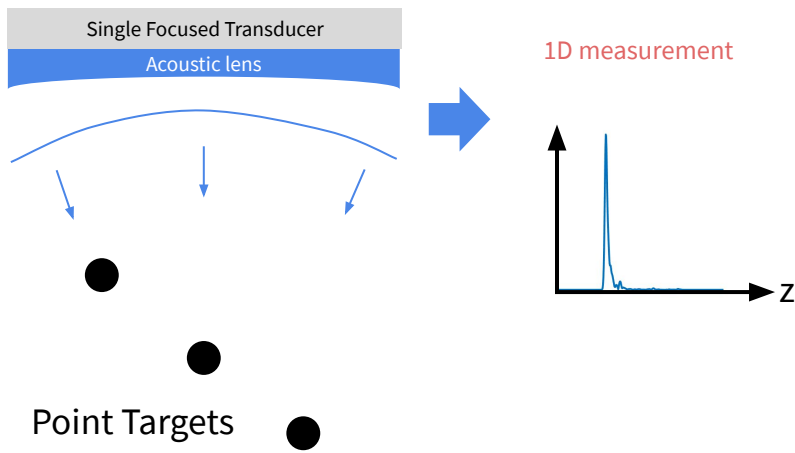
# Single Element Ultrasound Imaging with Compressed Sensing

William Meng  
EE 367 Final Project  
March 17, 2021

# Background

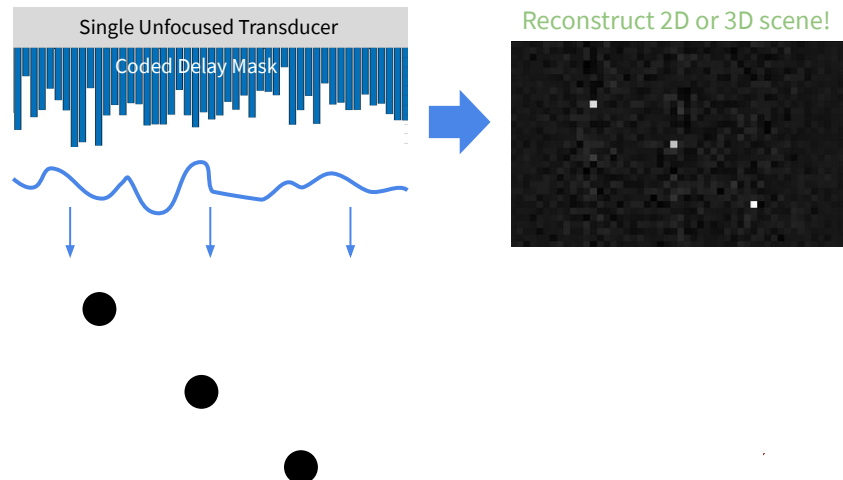
## Single Element Ultrasound Imaging (A-mode)

- Capture time-series data to measure depth information
- Time of arrival indicates depth of target
- No lateral information



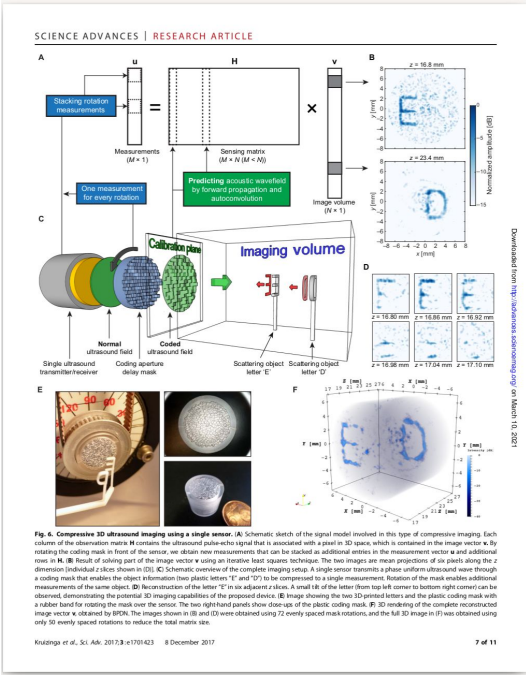
## Single Element Ultrasound Imaging with Compressed Sensing

- Use laterally-varying pseudorandom delay mask to encode lateral information into time-series data, in addition to the depth information already captured.



# Related Works

Kruizinga et al: “[Compressive 3D ultrasound imaging using a single sensor](#)”



Deán-Ben et al: “[Acoustic Scattering Mediated Single Detector Optoacoustic Tomography](#)”

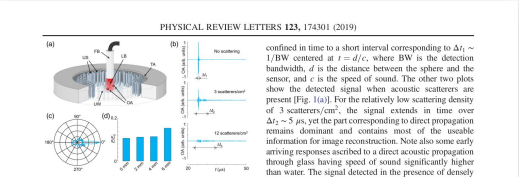


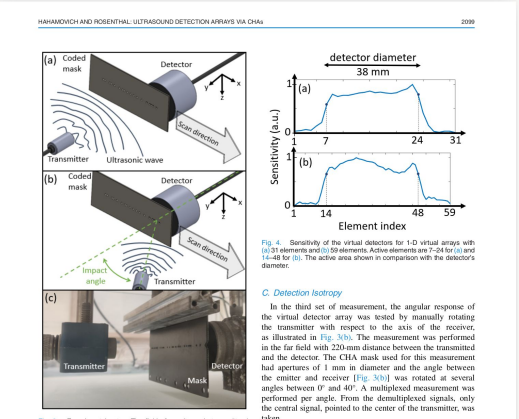
FIG. 1. Acoustic scattering of optoacoustic waves. (a) Layout of the experimental system. TA, transducer array; US, ultrasound scatters; FB, fiber bundle; LB, laser beam; OA, optical absorber. (b) Sensitivity of the virtual detector to 10.0 virtual amps with no scattering (top), with scattering density of 3 scatterers/cm<sup>2</sup> (middle), and with scattering density of 12 scatterers/cm<sup>2</sup> (bottom). For the relatively low scattering density of 3 scatterers/cm<sup>2</sup>, the signal extends in time over  $\Delta t = 5\ \mu s$ , yet the period corresponding to direct propagation remains dominant and contains most of the useable information for image reconstruction. Note also some early arriving responses ascribed to a direct acoustic propagation through glass, whose speed is significantly higher than water. The signal extends in the presence of densely distributed 12 scatterers/cm<sup>2</sup> exhibits a complex pattern spanning  $\Delta t = 10\ \mu s$  and has no dominant peaks. In this case, the location of the point about one centimeter along the entire masked interrogator may give distribution of optical absorbers can potentially be compressed into a single wavelength.

We have measured the diffraction pattern for an individual scatterer by placing an absorbing microscope at the center of the transducer array and a glass tubing at a distance of 16.25 mm from it. The relative amplitude of the scattered wave for different angles was estimated by measuring the amplitude of the signals collected by all the array elements with and without the tubing in the propagating path. Note that the scattering diffraction pattern is generally dominated by scattering wave from an incident plane wave. For the measurements performed, the distance between the absorbing microscope is much larger than the diameter of the glass tubing and, hence, the incident wave cannot be approximated as plane. It is shown that the scattered waves have a dominant forward propagation component. This is expected considering that the effective diameter of each scatterer corresponds to  $\sim 5\ \mu m$  at the maximum wavelength, the central frequency of the detection array, which falls in the Mie scattering regime. Forward propagation is essential to minimize the loss of energy due to transmission through the glass tube. Collecting signals with high energy is essential for both scattering wave detection as well as for achieving a good signal-to-noise ratio (SNR) in the recorded images. Figure 1(d) shows the ratio of the total detected (OA) wave to the total array elements with and without ( $E_{sc}$ ) scatters present in the propagating path. For our detection configuration approximately 10% of the OA signal is lost due to scattering, which is within the expected range. This is because the OA scatters located far away from the array's center, suggesting that cylindrical focusing of the detection elements contributes to the energy collection efficiency.

The effects of acoustic scattering in the collected OA signal are illustrated in Fig. 1(e). For a single-element diameter microphone (Cymetech LLC, Santa Barbara, CA), the signal detected by one of the array elements with a rubber band holding the mask over the sensor can be observed, demonstrating the potential 3D imaging capabilities of the proposed device. (E) Image showing the two 3D-printed letters and the plastic coding mask with a rubber band holding the mask over the sensor. The two right-hand panels show close-ups of the plastic coding mask and the 3D rendering of the complex reconstructed image. The two 3D volumes shown in (F) were obtained by 72 evenly spaced mask rotations, and the full 3D image in (F) was obtained using only 50 evenly spaced mask rotations.

The detection in the presence of acoustic scattering implies establishing a model linking the initial OA pressure (proportional to the optical absorption) to the collected pressure waveforms. Similarly to the time-domain

Hahamovich et al: “[Ultrasound Detection Arrays via Coded Hadamard Apertures](#)”



In the third set of measurement, the angular response of the virtual detector array was tested by scanning the receiver with respect to the axis of the receiver, as illustrated in Fig. 4(b). The measurement was performed in the far field with 220-mm distance between the transmitted and the detector. The CHA mask used for this measurement had a radius of 10 mm and a total diameter of 20 mm between the emitter and receiver [Fig. 4(b)]. The mask was rotated at several angles between 0° and 40°. A multiplexed measurement was performed per angle. From the demultiplexed signals, only the central signal, pointed to the center of the transmitter, was taken.

## IV. RESULTS

### A. Uniformity and Sensitivity

Fig. 4(a) and (b) show the relative sensitivity of each element in the array to the receiver for the case of  $N = 31$  and  $N = 59$ , respectively. The  $x$ -axis in Fig. 4(a) and (b), which represent the element index, was scaled by length to allow for a comparison between the results. The span of the array is 16.25 mm. The array size is 16.25 mm  $\times$  16.25 mm. For both masks, the length of the receiver, which was 8 mm, was smaller than lengths of the virtual detector array, which were 61.5 [Fig. 4(a)] and 59 mm [Fig. 4(b)]. As Fig. 4(a) and (b) show, the sensitivity of the array is very high for elements inside the receiver span. While one might expect that all the virtual detectors outside the span of the receiver would receive a zero signal, the results in Fig. 4(a) and (b) show that they receive a non-negligible signal outside the receiver span. This result may be attributable to diffraction. Because the aperture diameter is comparable with the acoustic wavelength, the transmission through the aperture is semisotropic [20].

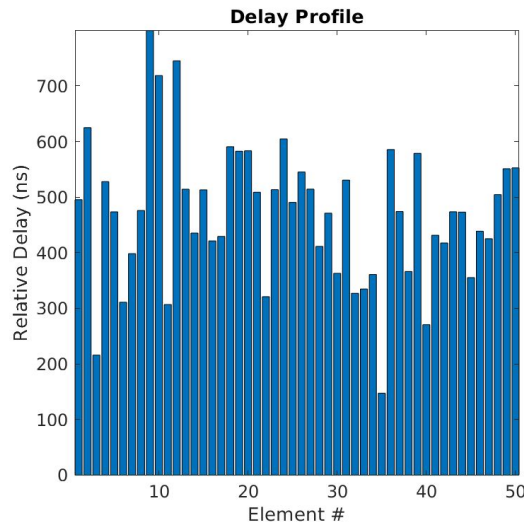
phase/delay mask

scattering layer

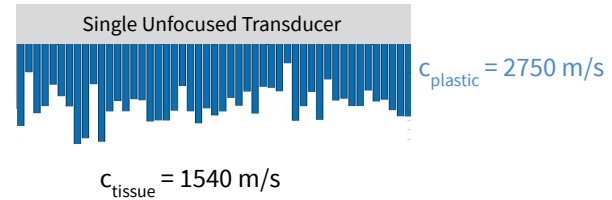
amplitude mask

# Approximating the mask as a delay profile

*Delay profile in simulation*



*Corresponding physical mask*



More complicated to simulate due to heterogeneity.

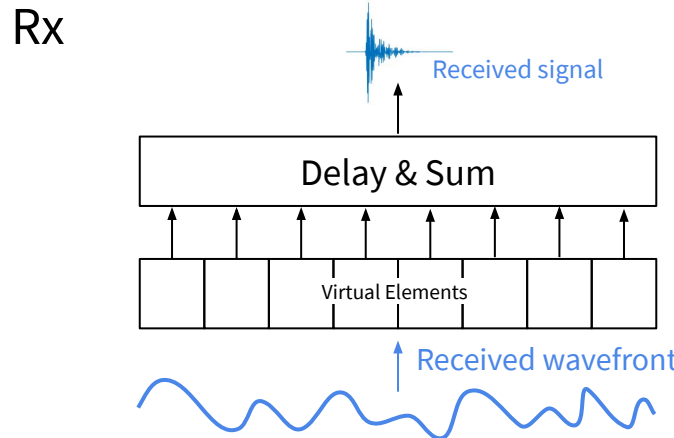
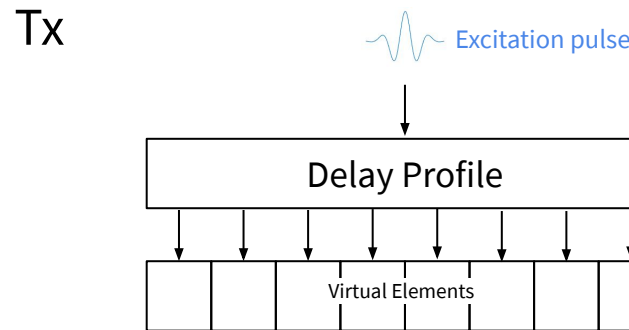
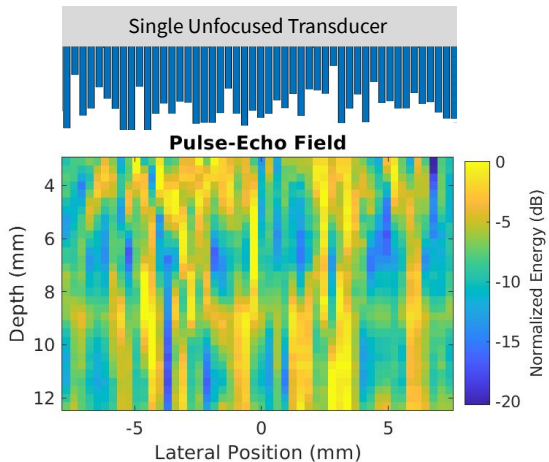
Ignores:

- Reflection at interface
- Refraction at interface
- Wave spreading within the mask

Much easier and faster to simulate!

# Ultrasound Simulation

Used *Field II* in Matlab to simulate pulse-echo response:



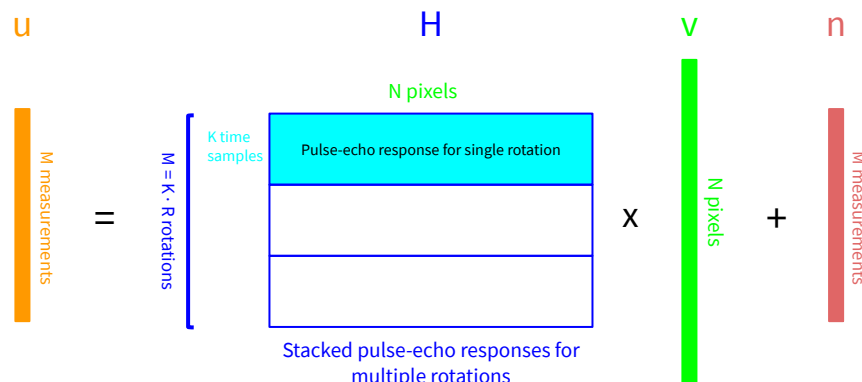
# Image Formation Model

Image formation model:

$$u = Hv + n$$

Where:

- $v$  = ground truth image
  - Size:  $(N, 1)$
- $H$  = image formation matrix
  - Size:  $(M, N)$
- $n$  = additive Gaussian noise
  - Size:  $(M, 1)$
- $u$  = measured data
  - Size:  $(M, 1)$



Dimensions:

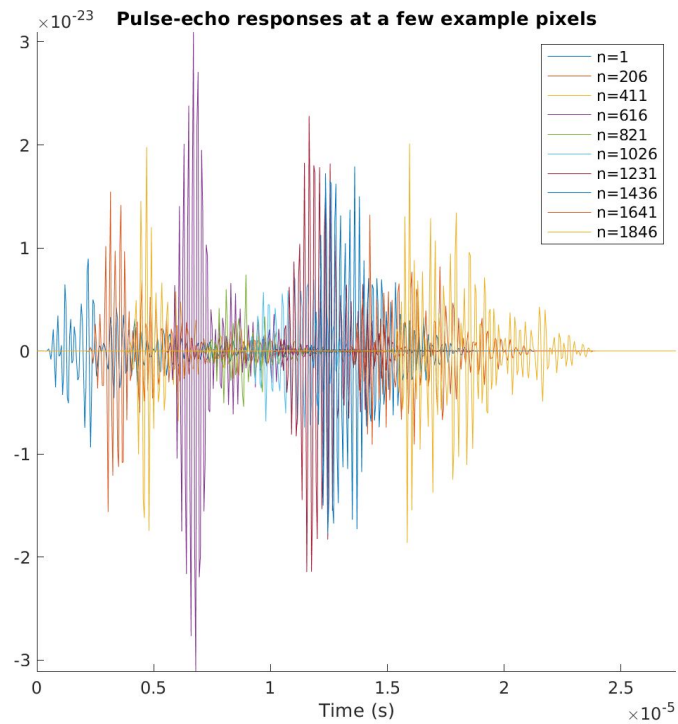
- $N$  = number of pixels in image
- $M = RK$  = number of measurements
  - $K$  = number of time samples in measured signal for each rotation
  - $R$  = number of rotations

# Example of some pulse-echo waveforms

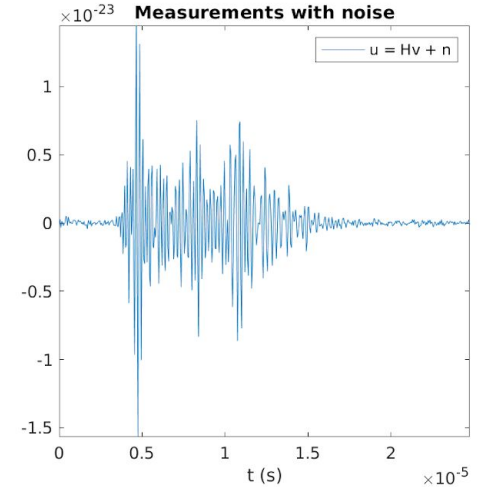
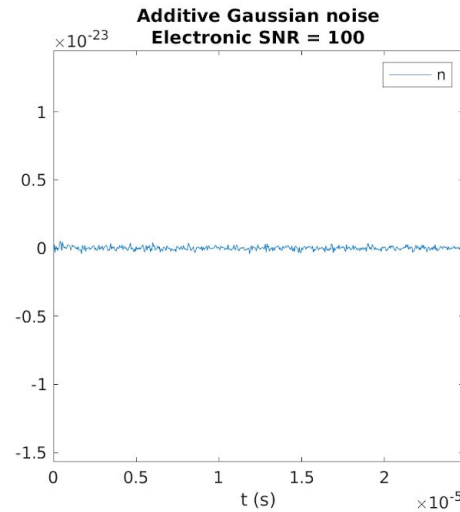
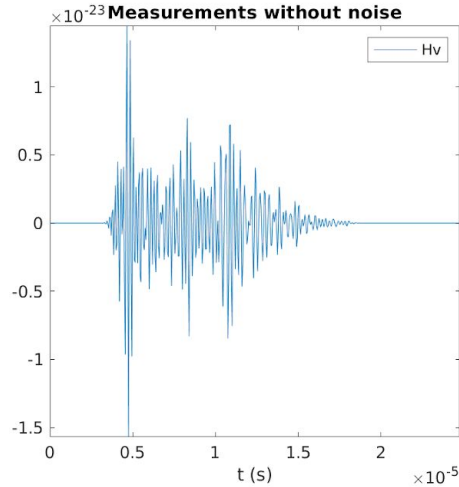
Each waveform shown here is the time-series data that represents the pulse-echo response for a pixel  $n$  in the field of view.

In the single rotation case, each column of  $H$  is just one of these waveforms.

In the multi-rotation case, each column of  $H$  is formed by concatenating the waveforms from each rotation.



# Example Measurement



# Reconstruction Algorithms

## *Least Norm Solution*

Problem:  $\min_{\hat{v}} \|H\hat{v} - u\|_2^2$

Solution:  $\hat{v} = H^T(HH^T)^{-1}u$

Implemented with:

- Preconditioned Conjugate Gradient (PCG)
- Moore-Penrose Pseudo-inverse

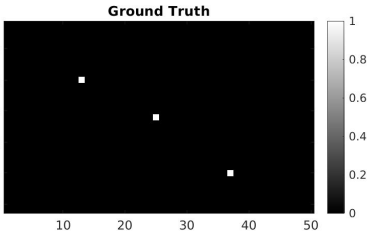
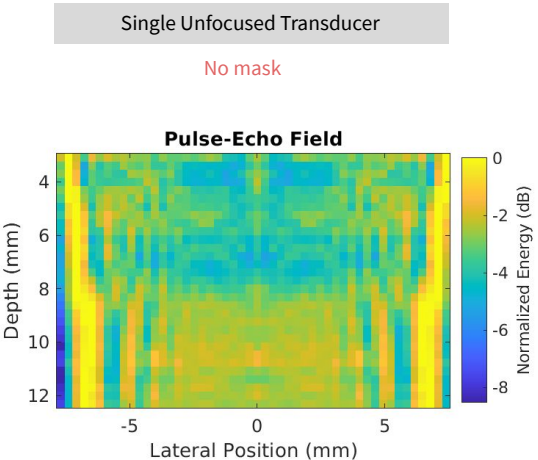
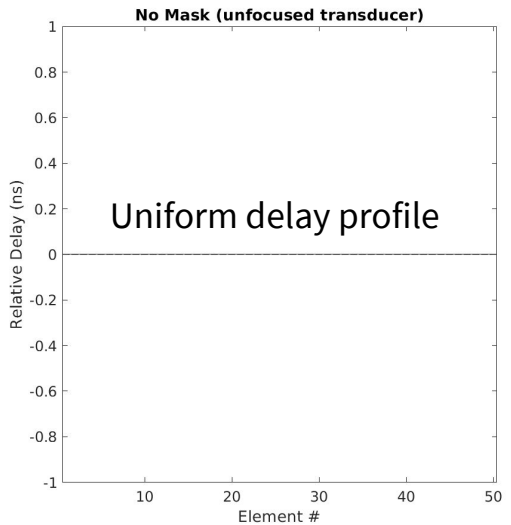
## *ADMM*

See EE 367 Lecture 11 notes for more details.

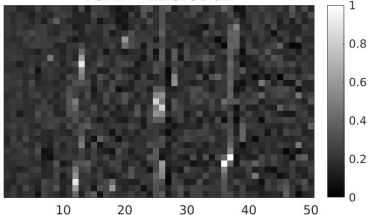
# Image Reconstruction (no mask)

The pulse-echo field with no mask actually does have some spatiotemporal diversity due to the near-field interference pattern of an unfocused transducer.

However, there are substantial artifacts in the reconstructed image due to the large amount of symmetry and self-similarity in the pulse-echo field. You can see erroneous “double point” targets in the reconstructed images, as well as a lot of background noise.



**Least Norm (PCG) Solution**  
 $\text{maxIterCG} = 1000$ ,  $\text{tolCG} = 1.20525e-32$   
 Runtime = 1.05212 s  
 PSNR = 12.6732 dB



**Least Norm (Pseudo-inverse) Solution**  
 $\text{tolPinv} = 0$   
 Runtime = 0.085966 s  
 PSNR = 17.7269 dB

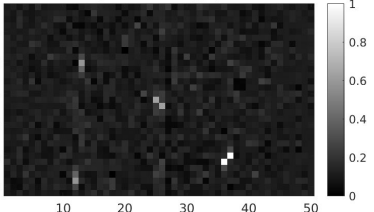
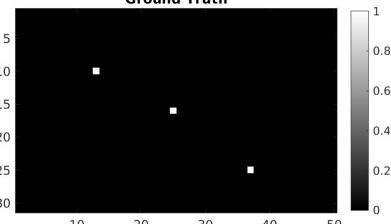
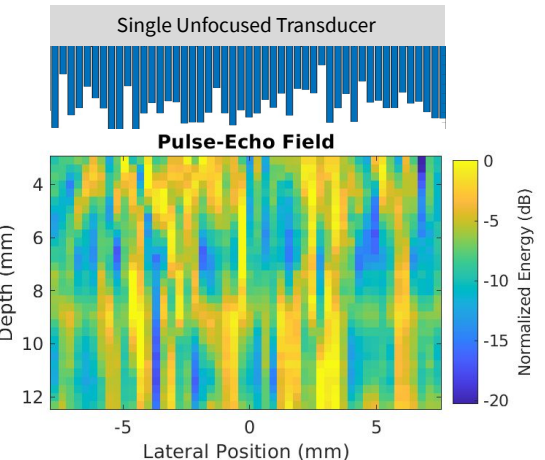
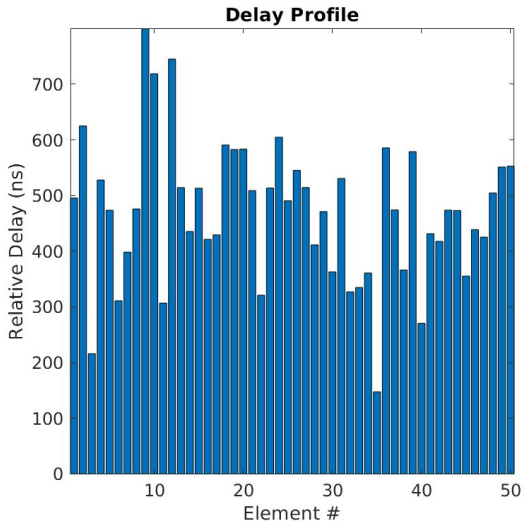


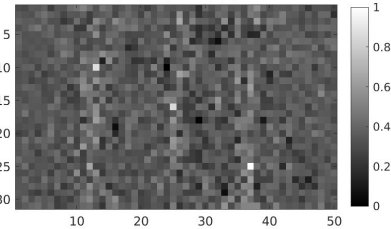
# Image Reconstruction (single rotation)

The pulse-echo field with a single rotation of the mask is highly aberrated and has little symmetry.

The reconstructed image resolves the 3 point targets with high spatial accuracy, but there are artifacts that appear as background noise, so the PSNR is actually worse than the “no mask” case.



**Least Norm (PCG) Solution**  
 $\text{maxIterCG} = 1000$ ,  $\text{tolCG} = 1.44731e-32$   
 Runtime = 1.15767 s  
 PSNR = 8.77796 dB



**Least Norm (Pseudo-inverse) Solution**  
 $\text{tolPinv} = 0$   
 Runtime = 0.094622 s  
 PSNR = 9.74446 dB

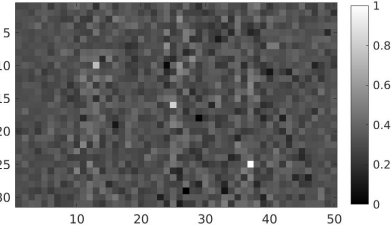
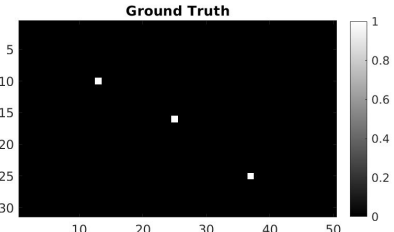
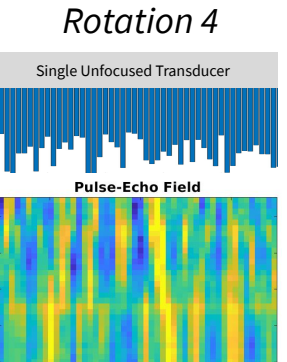
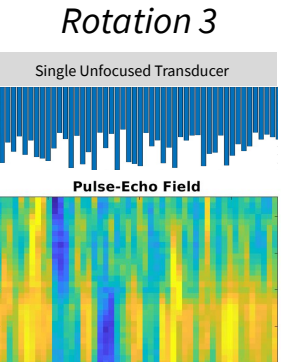
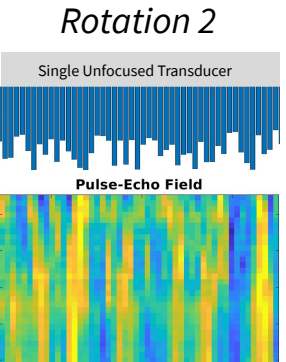
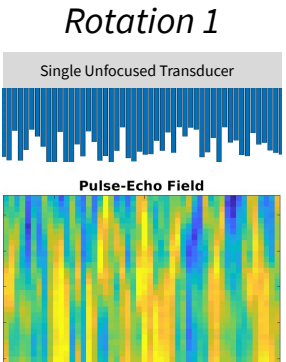


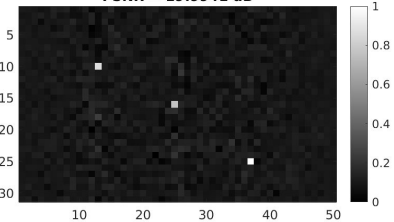
# Image Reconstruction (4 rotations)

Each rotation produces a completely different pulse-echo pattern, which captures more information about the scene.

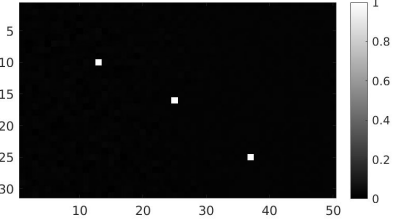
Very good image reconstruction quality, as indicated by high PSNR. Pseudo-inverse solution looks pretty much perfect.



Least Norm (PCG) Solution  
maxIterCG = 1000, tolCG = 3.98246e-32  
Runtime = 4.05171 s  
PSNR = 19.9941 dB

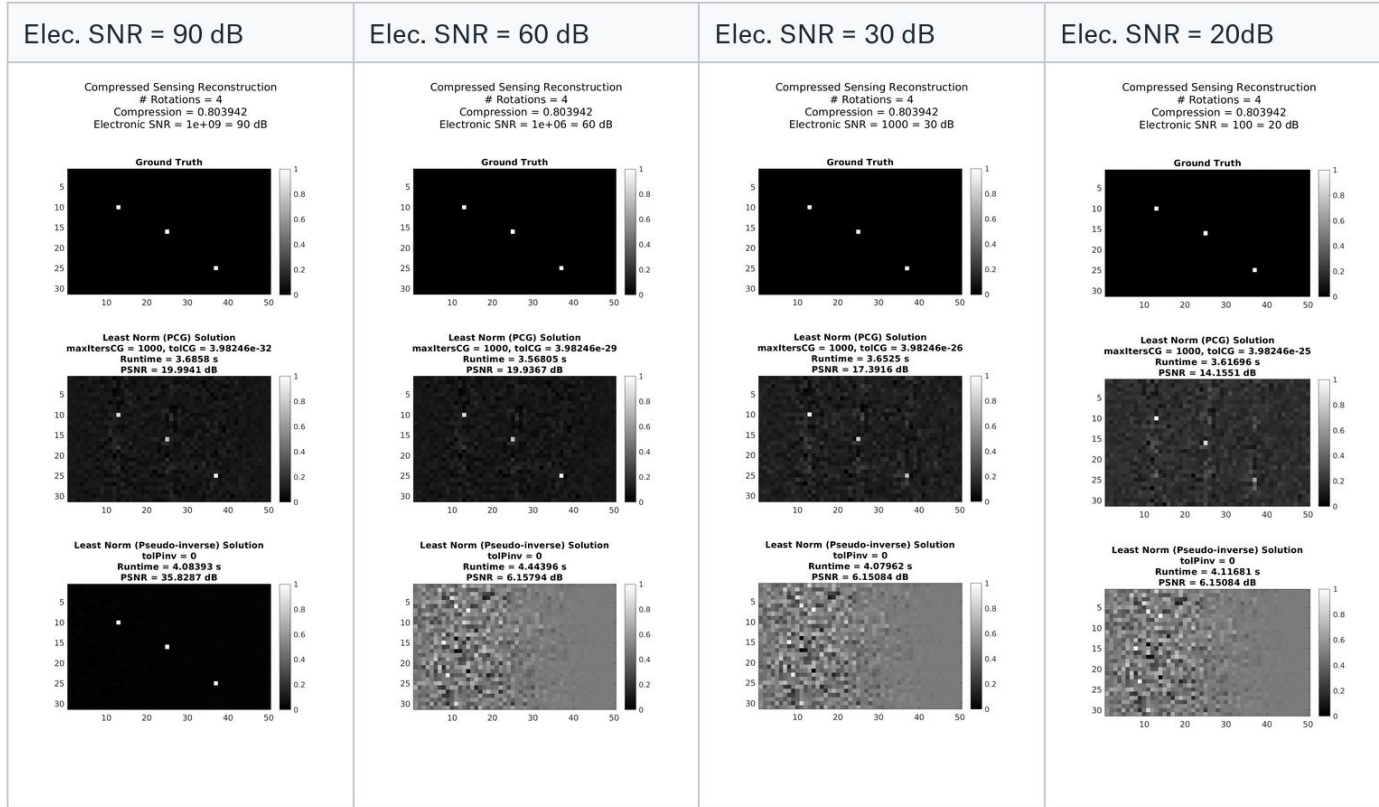


Least Norm (Pseudo-inverse) Solution  
tolPinv = 0  
Runtime = 4.46175 s  
PSNR = 35.8287 dB



# Impact of electronic SNR

(R=4 in all cases)



PCG image degrades gradually with electronic SNR.

Pseudo-inverse fails unless you have very high electronic SNR.

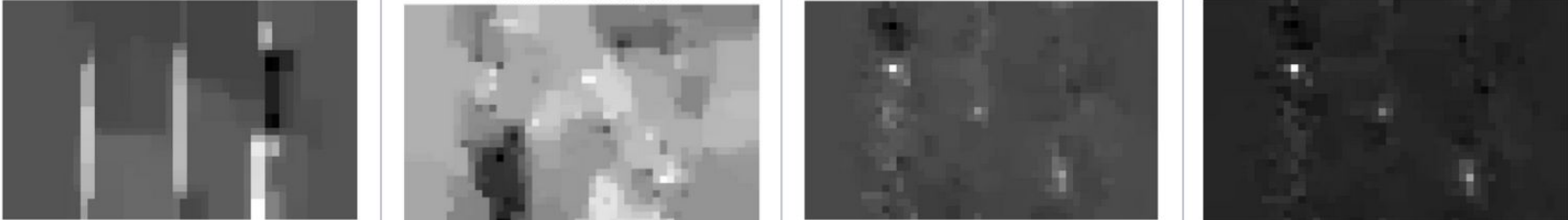
# ADMM with anisotropic TV regularization

ADMM ended up producing worse results than the Least Norm solutions.

Maybe there is an issue with the parameters I chose?

Or perhaps the TV regularizer doesn't work well for the scene with point targets?

No Mask	1 Rotation	4 Rotations	10 Rotations
$\lambda = 0.01, \rho = 10$ PSNR = 8.44859 dB Runtime = 9.7165 s	$\lambda = 0.01, \rho = 10$ PSNR = 3.91739 dB Runtime = 8.63383 s	$\lambda = 0.01, \rho = 10$ PSNR = 10.684 dB Runtime = 10.2342 s	$\lambda = 0.01, \rho = 10$ PSNR = 16.2542 dB Runtime = 14.8637 s



## Further work

- Image more complicated scenes.
- Use real-world ultrasound data instead of idealized synthetic data.
- Incremental reconstruction of a dynamic scene using a Kalman filter
  - Instead of simply taking an ensemble average of each individual reconstruction, iteratively combine the previous reconstruction with the new one based on statistical properties.
- Reconstruct a 3D volume
- Parallelize the reconstruction algorithm to run on a GPU
- Use a specifically designed mask like a Coded Hadamard Aperture

# References

[1] P. Kruizinga, et al, “Compressive 3D ultrasound imaging using a single sensor”, Science Advances, Vol. 3, No. 12, December 2017.  
<https://advances.sciencemag.org/content/3/12/e1701423>

[2] E. Hahamovich, A. Rosenthal, “Ultrasound Detection Arrays Via Coded Hadamard Apertures”, IEEE Transactions on Ultrasonics, Ferroelectrics, and Frequency Control, Vol. 67, Issue 10, Oct. 2020.  
<https://ieeexplore.ieee.org/document/9090912>

[3] X. Luís Deán-Ben, et al, “Acoustic Scattering Mediated Single Detector Optoacoustic Tomography”, Physical Review Letters, Vol. 123, Iss. 17, 25 October 2019.  
<https://journals.aps.org/prl/abstract/10.1103/PhysRevLett.123.174301>

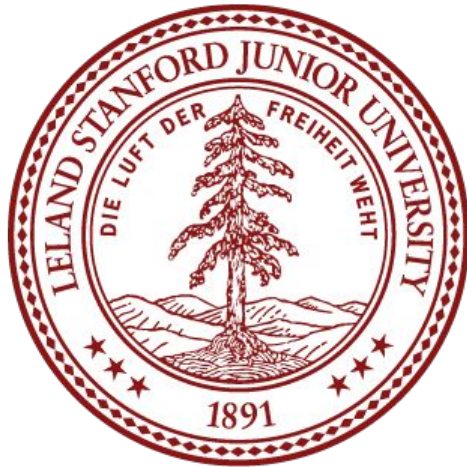
Code acknowledgments:

- Ultrasound simulation was performed using the [Field II](#) library in Matlab, with code adapted from the RAD 235 workshops.
- PCG and ADMM code was adapted from the EE 367 homework.

Thank you!

Please email me at [wlmeng@stanford.edu](mailto:wlmeng@stanford.edu) if you have any questions!

**Poster Version**



## Figures for Paper

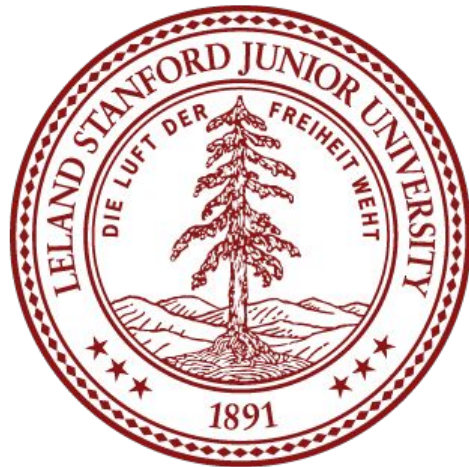
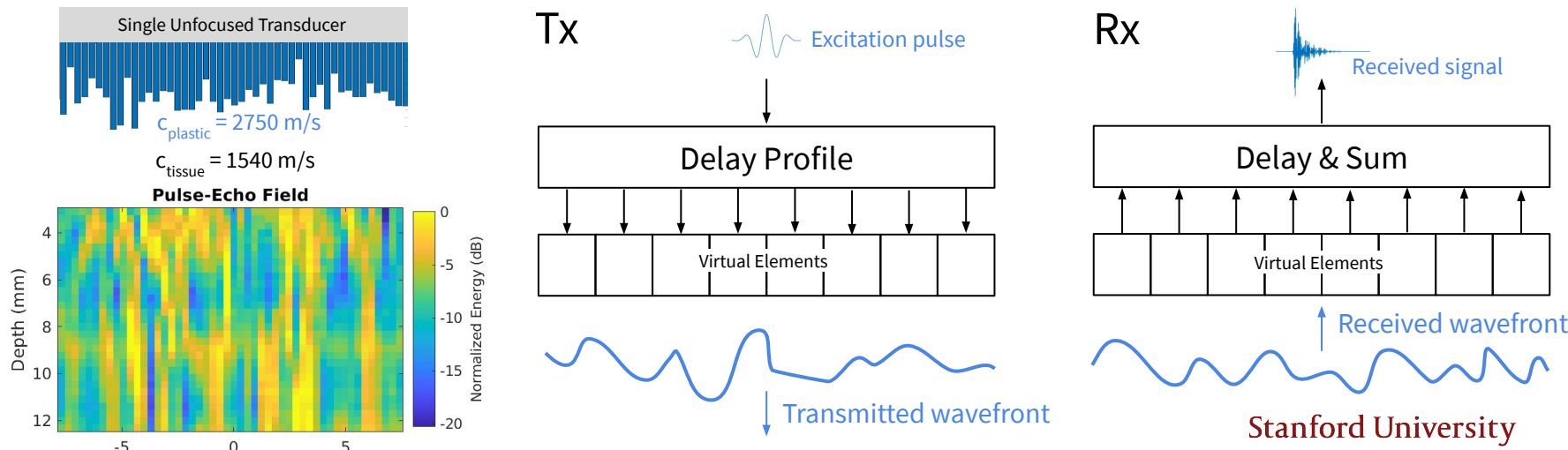
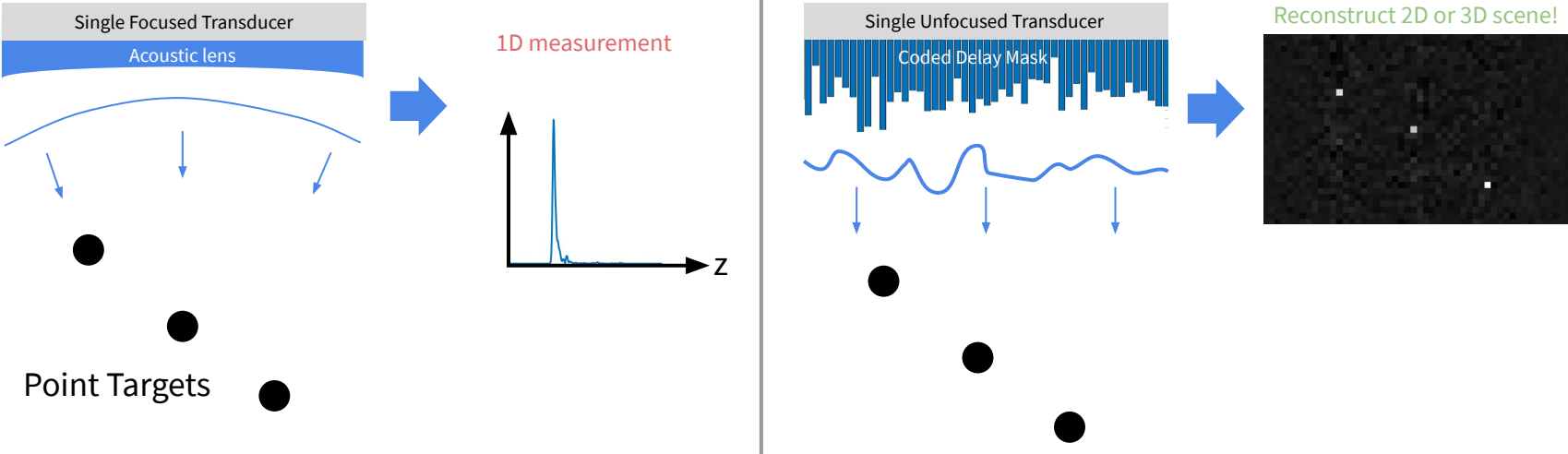
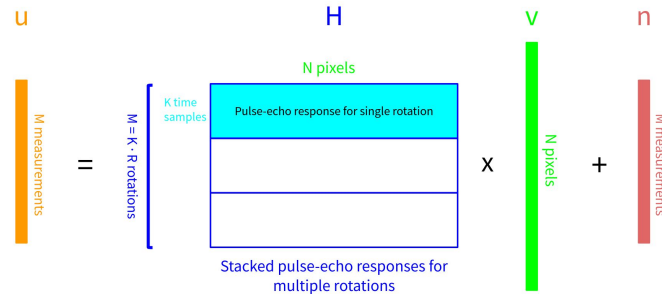


## Fig. 1

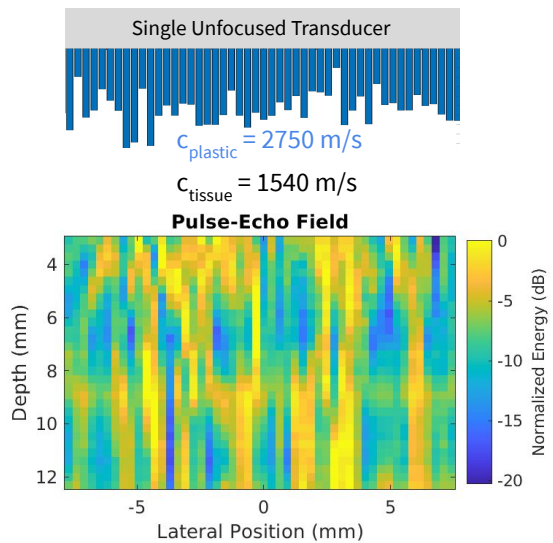
- a) A-mode
- b) compressed sensing
- c) physical mask → delay profile
- d) block diagram with virtual elements



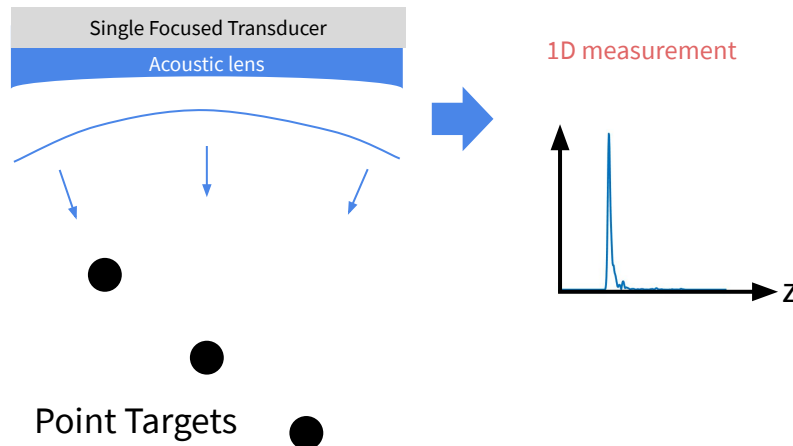
(a)



(b)



(a)



(b)

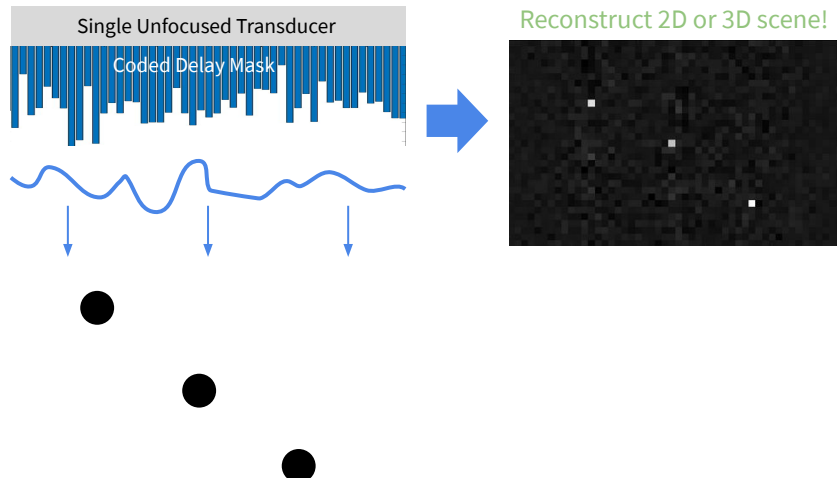


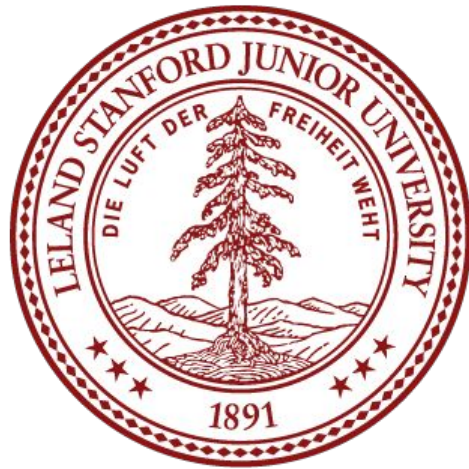
Fig. 2

Fig. 3

Fig. 4

Fig. 5

Archived



# Simulation Approach

Approximate delay mask as a near-field phase mask.

- Ignore amplitude
- Ignore reflection & refraction effects

In essence, each element in the mask will only affect the local delay on the transducer.

By using this approximation, we avoid simulating the wave propagation in the plastic material (which would require a finer grid size).

Instead, we perform the simulation in a homogeneous medium, which is computationally more efficient.

# Physical Representation vs. Simulation

## Physical

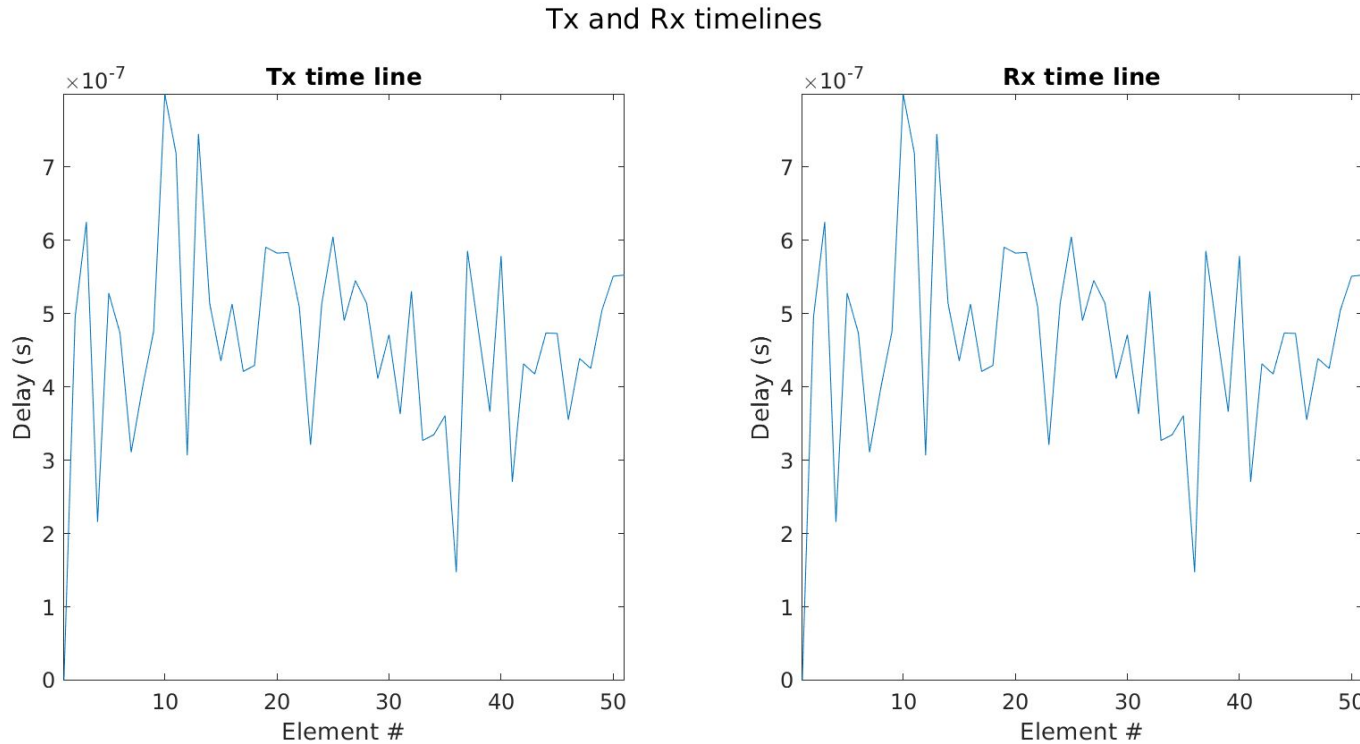
uniform wavefront from transducer, aberrations produced by propagation through delay mask

## Simulation

aberrations produced directly by delays applied to each element in transducer array summing across all elements

# Localized delays

In the simulation, we are defining a multi-element array for the sole purpose of emulating a physical delay mask. The “single sensor measurement” can be attained by averaging the signal measured by all the elements.



# True Image

True image

